ACS APPLIED MATERIALS & INTERFACES

Research Article

www.acsami.org

Influence of Hydrogen Annealing on the Photocatalytic Activity of Diamond-Supported Gold Catalysts

Sergio Navalon,* David Sempere, Mercedes Alvaro, and Hermenegildo Garcia*

Instituto Universitario de Tecnología Química CSIC-UPV and Departamento de Química, Universidad Politécnica de Valencia, Avenida de los Naranjos s/n, 46022 Valencia, Spain

Supporting Information

ABSTRACT: Fenton-treated diamond nanoparticles have been submitted to hydrogen reduction at 500 °C with the purpose of modifying the nature of the functional groups present on the diamond surface. The nature of the functional groups on the diamond samples was characterized by a combination of spectroscopic and analytical techniques. In particular, Fourier-transformed infrared spectroscopy, temperature-programmed desorption, and X-ray photoelectron spectroscopy (XPS) show the decrease in the population of carboxylic acids, esters, and anhydrides after hydrogen treatment. XPS also shows a decrease on the oxygen content after the hydrogen treatment of the diamond nanoparticles and lower electronegativity of the carbons as assessed by the lower binding energy values. Although Fenton-treated diamond colloids in water changes the zeta potential from positive to negative values as a function of the pH, hydrogen annealing and the disappearance of the carboxyl groups determines that the zeta potential of the resulting sample remains positive in the complete pH range. Deposition of gold nanoparticles was carried out by the polyol method consisting on the reduction of $HAuCl_4$ by hot ethylene glycol in the presence of the support. TEM analysis shows a variation of the average gold nanoparticle size that decreases after hydrogen reduction of carboxylic groups and becomes smaller for low gold loadings. The catalytic activity of the diamond supported gold nanoparticles as a function of the surface annealing treatment and gold loading was evaluated for the natural sunlight-assisted peroxidation of phenol by H_2O_2. It was observed that the most efficient sample was the one having lower gold nanoparticle size that was obtained for diamond samples reduced by hydrogen at 500 °C after the Fenton treatment and having low gold loading (0.05 wt %). Turnover frequencies above 2400 and 940 h^{-1} were obtained for phenol degradation and H_2O_2 decomposition, respectively.

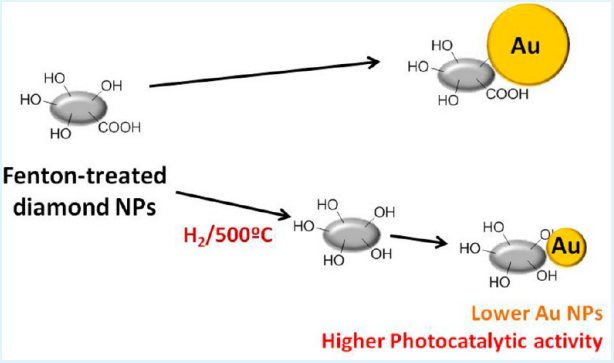

KEYWORDS: *diamond nanoparticles, gold supported, natural sunlight irradiation, heterogeneous photo-Fenton reaction*

1. INTRODUCTION

One of the most general methods to treat wastewaters is the Fenton reaction in which highly aggressive hydroxyl radicals (•OH) are generated by stoichiometric reduction of H_2O_2 by Fe(II) or other appropriate transition metal ions.[1−3] Because of the wide application of this process for the degradation of pollutants in water, there has been a continued interest in developing the catalytic version of this process in which after electron transfer the oxidized form of the metal ions is reduced by H_2O_2.[4−7] Although most of the solid catalysts that have been developed for this process are based on iron oxides supported on alumino-silicates[5] or carbon materials,[6] they tend to undergo extensive leaching under the reaction conditions. In this regard, we have reported that gold nanoparticles (NPs) supported on Fenton-treated diamond NPs (DF) is a highly efficient solid catalyst to effect the degradation of phenol by H_2O_2,[8,9] reaching an efficiency on •OH generation over 79%[9] and turn over numbers (TON) for phenol degradation above 458,000.[10] Previous studies comparing the activity of Au/DF with that of analogous materials in which Au NPs have been supported on metal oxides such as Au/TiO_2 have shown that these catalysts based on metal oxides exhibit much lower activity as Fenton promoters.[9,11] DF as support provides adequate surface functionalization to anchor Au NPs and at the same time is an inert support, leading to the formation of •OH radicals freely diffusing into the solution. For instance, •OH generated by photocatalysis on the surface of TiO_2 is known to form surface-bound •OH radicals in a large percentage.[12−14] Moreover, the system can be assisted by Solar light irradiation expanding the range of conditions in which this material is active.[11,15]

It has been observed that the catalytic performance of Au/DF strongly depends on the preparation conditions, the major problem being optimization of the experimental procedure in order to achieve the highest activity.[10] In the precedents, Au NPs were prepared by deposition-precipitation method that in addition of requiring long times has as drawback the waste of a

Received: April 24, 2013
Accepted: July 1, 2013
Published: July 1, 2013

large percentage of the starting gold that remains in the solution. In this regard, it would be of interest for the preparation of Au/DF to develop more convenient methods to generate and deposit Au NPs, such as the polyol procedure, which requires further optimization of the catalyst preparation.

In the present manuscript, we describe a new protocol for the preparation of Au/DF in which the optimization of the DF support as well as deposition of Au NPs by the solvatothermal reduction of Au(III) in hot ethylene glycol lead to an increase in the catalytic activity for the sunlight-assisted Fenton degradation of phenol by H_2O_2.

2. EXPERIMENTAL SECTION

2.1. Materials. H_2O_2 solution in water (30%, v/v), phenol (≥99%), HNO_3 (65%), HCl (37%, ACS reagent), H_2SO_4 (98%), $HAuCl_4{\cdot}3H_2O$, NaOH (ACS reagent), and diamond nanopowder (ref: 636444, 95%) were commercial samples from Sigma-Aldrich. Milli-Q water was used in all the experiments. The other reagents used were of analytical or HPLC grade.

2.2. Diamond Functionalization and Catalyst Preparation. Fenton-treated diamond NPs were obtained from commercial diamond (D) NPs as previously reported.[16] Basically, the reaction is carried out by suspending 0.5 g of D in 150 mL of H_2O_2 at pH 3 (H_2SO_4, 0.1 M) and adding dropwise for 2 h an aqueous solution of $FeSO_4 \times 7H_2O$ (2 g/30 mL) under sonication (420 W) in a water bath until the evolution of gases ceases. During this process ice has to be added to the bath to avoid the temperature to increase above 50 °C. A second cycle consisting in addition of 50 mL of H_2O_2 and again $FeSO_4 \times 7H_2O$ repeating the procedure was carried out with the treated D sample. Subsequently, the solid was collected and washed exhaustively first with acidic water at pH 3 (to avoid iron precipitation) and then with neutral water until pH 7. Finally, the resulting freeze-dried sample was denoted as DF. Additionally, the DF sample was submitted to a subsequent thermal annealing under continuous H_2 flow. Briefly, the DF sample was placed in a quartz reactor under H_2 flow (100 mL min^{-1}) and heated using a ramp of 8 °C min^{-1} up to 500 °C and the this temperature maintained for 6 h. Then, the sample was allowed to cool down at room temperature while the flow of hydrogen is maintained, the resulting powder labeled as DFH. Finally, a sample denoted as DFH_N_2 was obtained by heating DFH sample in a quartz reactor under N_2 flow (100 mL min^{-1}) using a ramp of 10 °C min^{-1} up to 700 °C and this temperature maintained for 30 min. The cool down at room temperature of the system was also carried out while maintaining the flow of nitrogen.

Preparation of Au/DF, Au/DFH and Au/DFH_N_2 catalysts was accomplished using the polyol method.[16−18] In particular, 200 mg of the support (DF, DFH or DFH_N_2) were suspended in 80 mL of ethylene glycol and sonicated for 30 min. Although this procedure can also be used for somewhat larger amounts of sample, the catalytic activity of resulting supported gold catalyst typically decreases significantly when the recipe is scaled up for larger weights of support and gold. Then, the corresponding amount of gold salt dissolved in water was added to the D suspension to achieve the required gold loading (from 0.05 to 0.5 wt %). The suspension was heated up to 85 °C under vigorous stirring and allowed to react for 4 h. After cooling the reaction at room temperature, the suspended powder was recovered by centrifugation at 14,000 rpm. Then, the supernatant was removed and the catalyst dispersed in ethanol and washed by performing three consecutive centrifugation−redispersion cycles with ethanol and acetone and three more using water. Finally, the catalysts (Au/DF, Au/DFH, and Au/DFH_N_2) were freeze-dried.

2.3. Characterization. Quantitative Fourier-transformed infrared (FT-IR) spectra of the different samples were recorded on a Nicolet 710 FTIR spectrophotometer by using KBr disks of the samples prepared pressing the wafers (10 mg) at 10 Ton × cm^{-2} for 2 min. Elemental analyses were measured using a Perkin-Elmer CHNOS analyzer. Solid-state ^{13}C NMR spectroscopy was recorded in a Bruker AV 400 instrument. Temperature-programmed desorption coupled to a mass-spectrometer (TPD-MS) was carried out in a Micromeritics II 2920 connected to a mass-spectrometer. In particular, TPD was carried out under helium using 100 mg of sample, heating from room temperature to 900 °C at 10 °C min^{-1}. X-ray photoelectron spectroscopy (XPS) measurements were performed on a SPECS spectrometer with a MCD-9 detector using a monochromatic Al (Kα = 1486.6 eV) X-ray source. Spectra deconvolution has been performed using the CASA software and binding energies were referenced to the C 1s peak at 284.4 eV.[19] Zeta potential measurements were carried out using a Zetasizer ZS nano (Malvern instruments, Germany). In particular, the zeta potential of aqueous suspension of D materials (10 mg L^{-1}) was determined adjusting at the required pH value using HCl (0.1 M) or NaOH (0.1 M). The specific Brunauer−Emmett−Teller (BET) surface area was measured using an ASAP 2010 Micromereitics apparatus.

Metal loading (0.05, 0.1, 0.25, and 0.5 wt %) on the D NPs was determined by inductively coupled plasma atomic emission spectroscopy (ICP-AES). The percentage of gold leached from the solid catalyst to the solution was determined also by ICP-AES analyses of the filtered samples (0.2 μm Nylon filters) at the end of the reaction. The detection limit of the technique was 0.1 mg L^{-1}. X-ray diffractograms (XRD) were recorded by using a Philips X-Pert diffractometer equipped with a graphite monochromator, operating at 40 kV and 45 mA and employing Ni filtered CuKα radiation (λ = 0.1542 nm).Transmission electron microscopy (TEM) and high resolution TEM (HRTEM) of the different samples were obtained using a TECNAI G2 F20 (FEI) instrument operating at 200 kV with a resolution of 0.24 nm. Dark-field scanning TEM (DF-STEM) measurements were performed using a JEOL JEM-2100F instrument operating at 200 kW. DF-STEM was also used in combination with X-EDS detector (Oxford Instrument) for microanalyses of Au NPs. The particle size distribution was estimated by counting more than 400 particles.

2.4. Photocatalytic Experiments. Catalytic experiments were carried out under natural sunlight irradiation and measuring the phenol disappearance and H_2O_2 decomposition. Briefly, 100 mL of aqueous phenol solution (100 mg L^{-1}) was placed in a 500 mL round-bottom flask. Then, the desired amount of the catalyst was added and the system sonicated for 10 min. Once the initial pH was adjusted at the value of 4 using aqueous solutions of HNO_3 (0.1 M) or NaOH (0.1 M), the samples were exposed to the sun and the required amount of H_2O_2 was added to start the reaction. During the reaction the pH value was maintained at pH 4 to minimize gold leaching from the heterogeneous catalyst to the solution. It was observed that evolution of phenol decomposition lowers significantly the pH of the solution and periodic additions of NaOH (0.1 M) are needed to correct the pH to maintain the value at 4. Keeping the pH value above 3 avoids gold leaching from the solid catalyst to the aqueous solution as previously reported.[9]

Time conversion of phenol was determined by analyzing aliquots (2 mL, filtered through 0.2 μm Nylon filter) by reverse-phase Kromasil-C18 column using H_2O/CH_3OH/acetic acid, 69:30:1, as eluent under isocratic conditions and employing an UV detector. The residual H_2O_2 was determined by 10-fold dilution of the reaction mixture and using $K_2(TiO)(C_2O_4)_2$ (Aldrich) in H_2SO_4/HNO_3 as colorimetric titrator. The solution was allowed to react for 10 min before monitoring the intensity at 420 nm.

Reuse experiments were performed recovering the catalyst at the end of the previous cycle by filtration through a 0.2 μm nylon membrane. The catalyst was washed with Milli-Q water at pH 10 and then rinsed with Milli-Q water in order to remove the excess of base and salts. It should be commented that washings with basic water were carried out in order to remove possible carboxylic acids formed as degradation products that could deactivate the gold catalyst.[8,20] The recovered catalyst was used for the next run with appropriate substrate and solvent. When studying the reusability, the samples are submitted to natural sunlight solar irradiation that can vary on a daily basis. Therefore, catalytic experiments of the fresh and used samples were carried out simultaneously.

Scheme 1. General Preparation Procedure for DF, DFH, and DFH_N$_2$ Supports

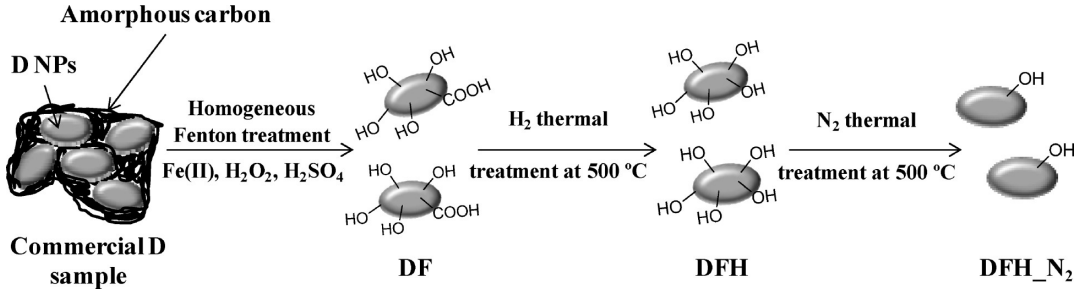

Quenching experiments using dimethyl sulfoxide (DMSO) as selective •OH radical quencher were carried out by adding DMSO to the reaction at a DMSO-to-H_2O_2 molar ratio of 10.[15]

Sunlight intensity was measured using a photodiode connected to a voltmeter. On average, the solar irradiation was 80 ± 18 mW cm^{-2} during the experiments performed in this study. Ambient and solution temperatures were, on average, 30.6 ± 2.6 and 26.9 ± 1.8 °C, respectively.

3. RESULTS AND DISCUSSION

3.1. Catalyst Preparation. Starting from commercial D NPs the Fenton treatment is applied to mineralize the amorphous soot matter embedding commercial D NPs and causing their agglomeration.[9] The chemistry of active carbons and other carbonaceous materials make ample use of oxidative treatments, particularly with HNO_3, to alter the surface functional groups.[21] We have previously shown that, in addition to the mineralization of the soot matter, oxidative Fenton treatment produces the appearance of hydroxyl groups on the surface but also some carboxylic groups.[9] We speculate that the presence of these carboxylic groups can have some effect on the deposition of Au NPs, altering the average particle size. To decrease the population of these carboxylic groups, we further submitted the DF sample to H_2 annealing at 500 °C to effect the reductive decarboxylation of these groups. This temperature was selected considering that TPD information (see below) indicates that substantial decomposition of carboxylic acid groups takes place and also that H_2 becomes strongly reducing agent under these conditions.[22] Considering that H_2 does not adsorb significantly in the majority of the solids, it is not expected that H_2 becomes physiadsorbed on D. However, H_2 could react with unsaturated multiple C−C and C−O bonds accessible on the surface of the material.[22] Scheme 1 summarizes the preparation procedure of the D supports that have been employed in the present study.

It should be commented that surface modification by Fenton and generation of oxygenated functional groups at the surface is specific for carbon containing materials such as D, whereas inorganic metal oxides such as TiO_2 do not behave similarly under similar conditions. Specifically, it has been reported that H_2 annealing at 500 °C of TiO_2 can lead to the formation of oxygen vacancies and generation of Ti^{3+} without affecting the increase in −OH density.[23]

The samples (DF or DFH) were subjected to characterization in order to gain insight into the functional groups present on the surface according to the treatment employed in the preparation. Figure 1 shows the FT-IR spectra of the samples under study.

FT-IR spectrum of the commercial D sample shows some weak bands at 3442 cm^{-1}, with the absence of high frequency carbonyl peak being notable and only weak C═O stretching

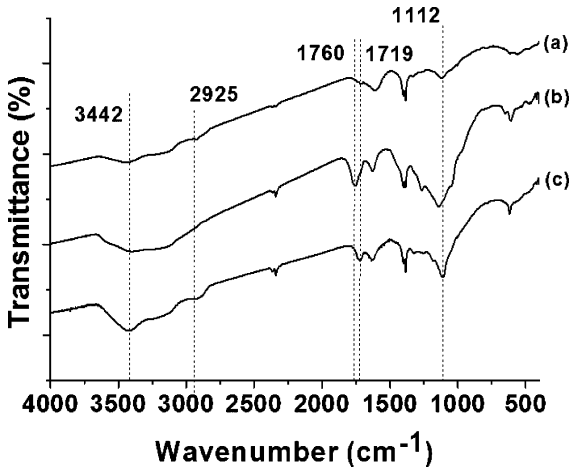

Figure 1. FT-IR of (a) commercial D, (b) DF, and (c) DFH samples.

vibration at 1719 cm^{-1}. According to the reported data,[9] Fenton treatment increases considerably the intensity and area of the −OH groups in the region from 3600 to 2900 cm^{-1} that are accompanied by the appearance of a new C═O band at 1760 cm^{-1} and also by an intensity increase of the low frequency C═O peak at 1719 cm^{-1}. As anticipated according to Scheme 1, H_2 annealing at high temperature changes the shape of the −OH vibration band that has now a defined maximum at 3442 cm^{-1} in the zone characteristic of alcohol −OH groups. In addition, development of C−H stretching band at 2925 cm^{-1} is clearly observed. These changes in the −OH region are accompanied by a diminution of the 1760 and 1719 cm^{-1} C═O bands corresponding to ester, lactones, carboxylic acids, and derivatives.[21]

The changes commented above for the FT-IR spectra depending on the D treatment can also be monitored by solid-state ^{13}C NMR spectroscopy. Figure 2 shows the set of magic angle spinning ^{13}C NMR spectra for the D samples. While block decay (BD) spectra of the three samples show predominantly a single peak corresponding to the core carbons appearing at 34.9 ppm, heteronuclear (^{1}H, ^{13}C) cross-polarization enhances the intensity of the signal corresponding to those carbons having hydrogen atoms in their neighborhood. As it can be seen there, the Fenton treatment of commercial D increases the intensity of the peak at 70.0 ppm that can be attributed to carbons in the alkoxy rest of esters or lactones. Also, the shape of the core carbons changes, particularly in the low field region at 50.1 ppm attributable to ethers and alcohols. When the DF sample is submitted to H_2 thermal annealing, the ^{13}C NMR peak at 70.0 ppm almost disappears completely in agreement with the decrease of the 1760 cm^{-1} band in the FT-

dx.doi.org/10.1021/am401489n | ACS Appl. Mater. Interfaces 2013, 5, 7160−7169

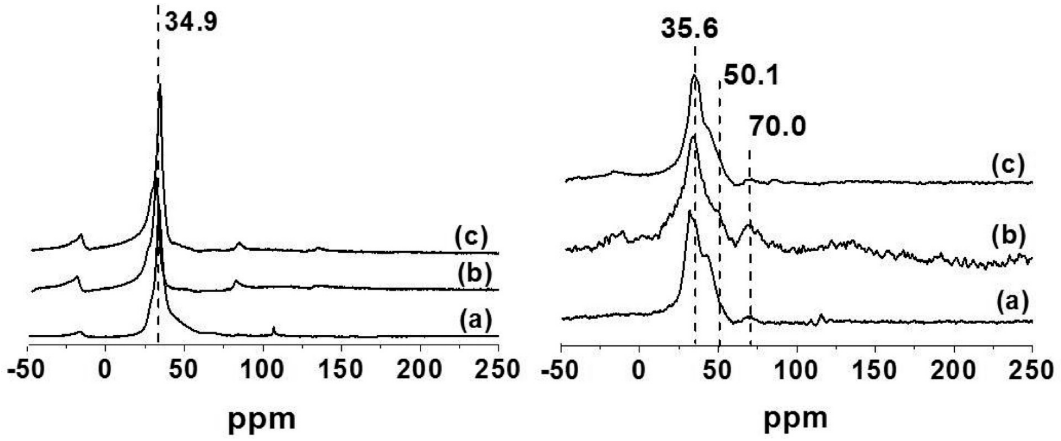

Figure 2. ^{13}C NMR spectra of (a) commercial D, (b) DF, and (c) DFH samples. Left, block decay; right, cross-polarization.

IR spectrum. Also, the intensity of the signal at 50.1 ppm decreases significantly.

Chemical analyses (Table 1) show that Fenton treatment increases by 5.1 wt % the percentage of oxygen in the sample in detriment of the percentage of elemental carbon that decreases in a similar proportion. This is compatible with Fenton process effecting partial oxidation of the material mainly on the surface, as it is observed by FT-IR and ^{13}C NMR spectroscopies. When the DF sample is annealed under a H_2 flow, then, chemical analysis reveals the opposite effect, i.e., a decrease in the percentage of oxygen and similar increase in the carbon content. These changes in the composition of the DF and DFH materials are in agreement with the expected chemical processes for H_2 annealing at high temperature consisting on decarboxylation and hydrogenation of multiple bonds. However, surface area values for the DF and DFH samples remain similar to that of commercial D NPs (Table 1).

Table 1. Elemental Analysis and S_{BET}[a] of Commercial and Treated D Supports[b]

	N (%)	C (%)	H (%)	O_2 (%)	H/C molar ratio	S_{BET} ($m^2\ g^{-1}$)
commercial D	2.5	89.1	1.0	7.5	0.13	273.1
DF	2.2	84.8	0.5	12.6	0.07	282.5
DFH	2.3	87.5	0.7	9.5	0.1	286.1

[a]Specific Brunauer–Emmett–Teller surface area (S_{BET}) [b]The experimental error of chemical analyses and surface area measurements are ±0.01% and 0.1 $m^2\ g^{-1}$, respectively.

TPD is a widely used technique that allows determining the nature of the oxygenated sites in carbonaceous materials.[21,24] It is expected that annealing under H_2 or N_2 atmosphere would lead the same level of CO_2 and CO decomposition. Upon heating, gradual decomposition of the oxygen-containing groups leading to CO_2 (carboxylic acids, ester, lactones, and anhydrides) and CO (ether, alcohols, ketones and quinones) is observed and depending on the decomposition profile, the distribution among possible oxygenated groups can be discussed. Figure 3 shows the TPD profiles of commercial D, DF, and DFH as well as the individual contributions of CO_2 and CO.

It can be seen in this Figure 3 that commercial D exhibit a low degree of CO_2 and CO evolution, indicating that this material contains a minor percentage of oxygenated groups. Upon Fenton treatment of this sample, DF exhibits a remarkable increase in the total gases evolved. Individual CO_2 and CO profiles for DF show that CO_2 desorption appears as a broad band from 300 to 700 °C, peaking at 650 °C. This high decomposition temperature indicates that the sample contains a relatively higher proportion of anhydrides, esters and lactones respect to carboxylic acids.[21] CO evolution exhibits a much narrower peak with a maximum at about 730 °C that we attribute mostly to the decomposition of surface hydroxyl groups introduced by the Fenton treatment. The DFH sample exhibits again a distinctive TPD profile where CO_2 evolution has been considerably reduced and only a sharp CO peak evolution, although somewhat less intense, remains. This variation in the TPD profiles nicely agrees with the chemical transformations taking place on the surface of D NPs upon the consecutive chemical treatments. Thus, Fenton oxidation should increase the oxygen content of the sample by producing many of the possible oxygenated functional groups including carboxylic acids and esters as well as anhydrides and hydroxyl groups. Chemical reduction with H_2 at 500 °C decreases the population of carboxylic groups and only alcohols and ethers should remain, this being in accordance with the almost exclusive evolution of CO.

XPS is also a very informative technique to investigate and address the type of carbons and functional groups present in carbonaceous materials.[24−26] Figure 4 shows the XPS peaks corresponding to C 1s and O 1s for the samples DF and DFH. This technique clearly reveals notable differences between these two samples as consequence of the thermal treatment under H_2. Thus, the peak intensity corresponding to O 1s that is a quantitative measure of the oxygen content of the sample, decreases significantly (about 45%) for DFH compared to DF. This decrease in the oxygen content determined by the reduction of the O 1s peak area is accompanied in the C 1s peak by a shift in the binding energy of the sample from 287.0 to 286.0 eV, reflecting that the overall environment of the carbons has became less electronegative as consequence of the lower oxygen content. Figure S1 in the Supporting Information shows deconvolution of the C 1s and O 1s XPS peaks providing more detailed information.

Another interesting property that is related to the nature of the surface functional groups and provides an idea of the stability of colloidal suspensions of D samples in water is the zeta potential. Herein, we have determined the influence of the pH on the zeta potential value for the D supports. Figure 5 presents the plot of zeta potentials versus pH for the samples.

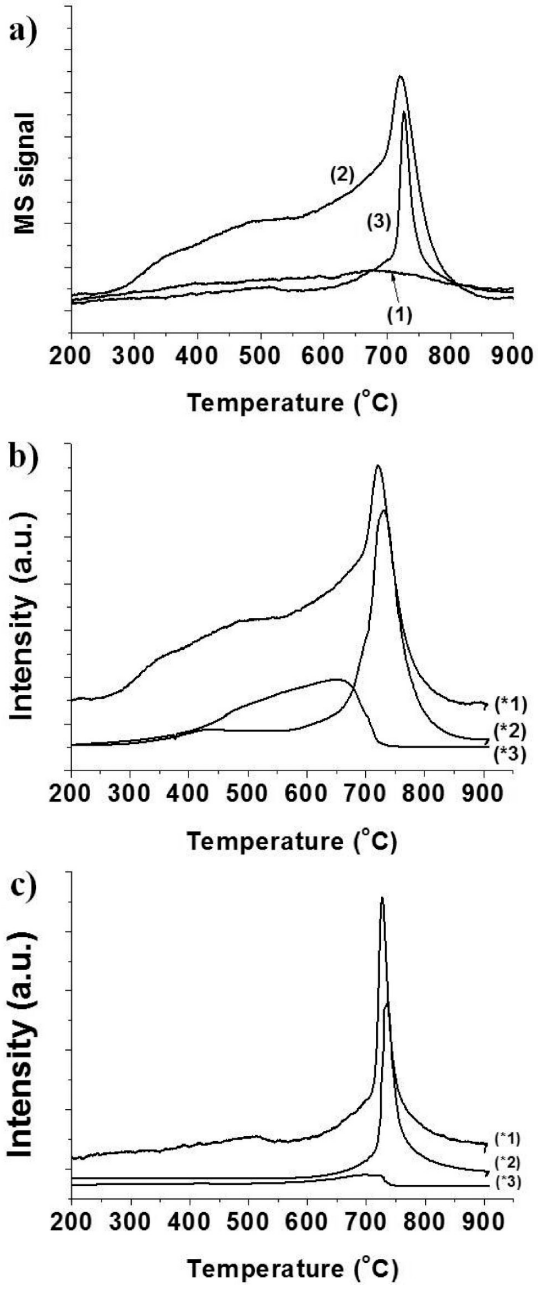

Figure 3. (a) TPD of (1) commercial D, (2) DF, and (3) DFH samples; (b) TPD-MS of DF sample; (c) TPD-MS of DFH sample. Legend: (*1) total gases; (*2) CO; (*3) CO_2.

As can be seen there, commercial D NPs have positive potentials in the range from 3 to 8 pH units. Importantly, after Fenton treatment the sample DF changes the sign of the zeta potential from high positive values at low pH to high negative values at basic pH. The point of zero zeta potential value was found about pH 4.8. This zeta potential profile for DF samples can be easily interpreted considering the prevalent role of carboxylic groups on the Coulombic charges on the surface. In this way, at pH values higher than 4.8, carboxylic groups in water will be present as carboxylates and, consequently, the surface should be negatively charged beyond this pH value corresponding to the pK_a of aliphatic carboxylic acids. At pH values below 4.8, these functional groups should be present in the acid form and the surface would become positively charged. The zeta potential profile determined for the DFH sample also agrees with the chemical reduction of carboxylic acids on the surface and, accordingly, colloidal aqueous suspensions of this DFH material show positive zeta potential values all over the pH range indicating that no carboxylic acids remain on the surface.

3.2. Au NP Deposition. Au NPs were deposited on DF and DFH samples using the conventional solvatothermal reduction of Au (III) in ethylene glycol.[16] Initially, the weight percentage of Au was 0.5 wt % but for the DFH support three additional samples with lower Au loading (0.05, 0.1, and 0.25 wt %) were also prepared since, as we will comment later, the photocatalytic activity using DFH as support was found higher than that of DF as support.

The different gold catalysts were first characterized by powder XRD. As it can be seen in Figure 6, all the catalysts exhibits the diffraction peaks corresponding to the D NPs appearing at 43 and 75°.[8] In addition, the Au(0.5%)/DF, Au(0.5%)/DFH and Au(0.25%)DFH catalysts also exhibits the characteristic gold diffraction peaks for the facets (111), (220) and (311).[27] Interestingly, the gold peak intensity decreases and becomes broader as a function of both H_2 annealing treatment of the DF sample (Figure 6a, b) and of the gold loading decrease (Figure 6c). We attributed these two effects to a decrease of the gold average particle size. In agreement with this interpretation, estimation of the gold particle size by applying the Scherrer equation leads to 9.4, 5.3, and 3.9 nm for the Au(0.5%)/DF, Au(0.5%)/DFH, and Au(0.25%)DFH catalysts, respectively. These observations, i.e., variation in the gold average particle size, the beneficial influence of H_2 annealing treatment and low gold loading to obtain small Au NPs, are also in good agreement with the measurements from TEM, HRTEM, and DF-STEM (see below). These microscopy techniques also allow characterization of the Au NPs supported on the Au(0.1%)/DFH and Au(0.05%)/DFH samples that due to the low Au loading do not exhibit the characteristic gold diffraction peaks in XRD (Figure 6d, e).

The presence of Au NPs on the different samples was also verified by means of microanalysis using a X-EDS detector (see Figure S2 in the Supporting Information). Figure 7 shows representative DF-STEM and TEM images as well as histograms showing the particle size distribution of Au NPs determined by counting about 400 individual particles. Figures S3 and S4 in the Supporting Information provides a more complete set of TEM and DF-STEM images. As a general rule and in accordance with the general trend observed for other supports,[28,29] a decrease in the Au loading leads to a decrease in the average particle size as well as a narrower distribution of the sizes. The most important feature from this TEM study was that DF as support renders Au NPs of 8.8 nm average size that is significantly larger than the mean diameter of 5.2 nm determined for DFH. This decrease in the average particle size can be accounted for considering that the nature of the surface functional groups is very important to control the growth of Au NPs. This study indicates the benefits of the thermal treatment with H_2 to remove carboxylic acid groups from the surface while still leaving surface hydroxyl groups to anchor Au NPs. Also, lower gold loadings as 0.25, 0.1, and 0.05 wt % resulted in an average gold particle size of 4.2, 3.8, and 3.4 nm, respectively. It should be, however, commented that measurements of average particle size based on TEM are always biased toward larger sizes because large particles are more clearly seen than the small ones or than clusters of a few gold atoms that are

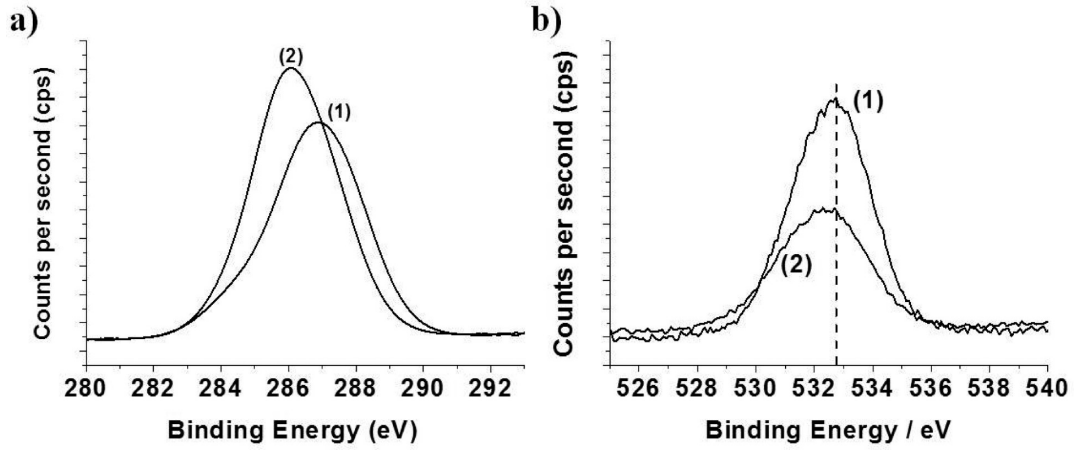

Figure 4. XPS spectra of (a) C 1s and (b) O 1s of (1) DF and (2) DFH supports.

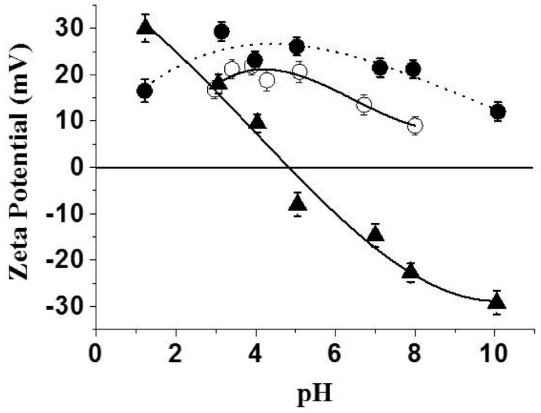

Figure 5. Zeta potential of commercial and treated D supports as a function of the pH. Legend: (○) commercial D, (▲) DF, (●) DFH. The error bars have been estimated from two independent experiments.

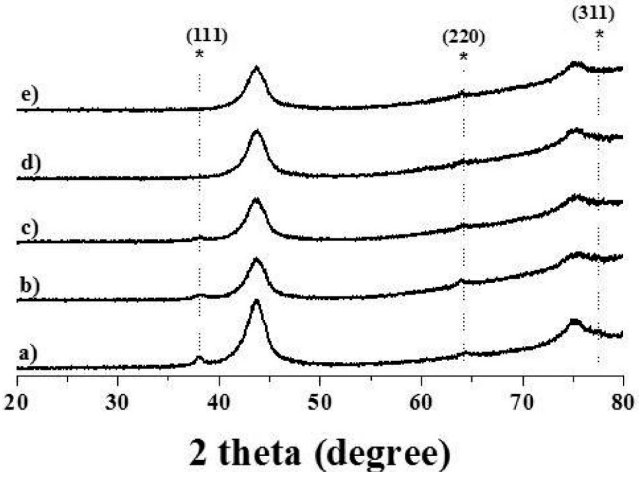

Figure 6. XRD diffractograms of (a) Au(0.5%)/DF, (b) Au(0.5%)/DFH, (c) Au(0.25%)/DFH, (d) Au(0.1%)/DFH, and (e) Au(0.05%)/DFH. The peaks labeled with asterisks correspond to characteristic Au diffraction peaks for the facets indicated in the plot.

difficult to be observed. The average Au NPs particle size distribution is relevant in catalysis considering that this parameter plays a high influence on the catalytic activity, with smaller-sized Au NPs being more active than larger Au NPs.

3.3. Photocatalytic Experiments. The natural solar-light-assisted catalytic activity of the Au/D catalysts prepared in this study was assessed for the peroxidation of phenol by H_2O_2 at pH 4. In the past, we have already used this reaction as a benchmark to evaluate the catalytic activity of various Au supported catalysts[9,11] and we have shown that visible light can enhance considerably the activity of the Au catalyst in this decomposition process.[11,15] The purpose of the present work was to assess if the activity of D supported Au NPs can be further increased by H_2 annealing of the Fenton-treated D support to favor the interaction with of D surface with Au NPs.

The time conversion plots for phenol degradation and H_2O_2 decomposition for the different materials studied are presented in Figure 8. It is important to note that in these experiments the H_2O_2-to-phenol molar ratio is 5.5 and even with this low H_2O_2 excess, the temporal profile of H_2O_2 is almost parallel to that of phenol degradation. Moreover, as can be seen in this figure, in some cases at final reaction times in where phenol has completely disappeared, some residual amount of H_2O_2 still remains at the final time. This indicates that our catalyst does not decompose spuriously large amounts of H_2O_2 and is very efficient for the generation of $^{\bullet}OH$ radicals. It should be commented that in the state of the art in heterogeneous Fenton catalysis it is not uncommon to use H_2O_2-to-phenol molar ratios above 1000, more than 2 orders of magnitude higher than in the present study using Au/D catalysts.

If the initial reaction rate for both processes, i.e., phenol degradation and H_2O_2 decomposition, is determined from the time conversion plots and, then, the turn over frequency (TOF) values that correspond to the number of catalytic cycles per Au atom in the fresh catalyst is determined, then, the relative activity of the different materials can be quantitatively ranked. Figure 9 presents the TOF values for the Au catalysts under study. From this figure, it can be concluded that Au NPs supported on the DFH sample at the lowest Au loading (0.05 wt %) is the most efficient catalyst according to this parameter. This higher activity of Au/DHF (0.05%) correlates directly with the smaller average particle size distribution of Au NPs in this support. However, we notice that this average particle size distribution of Au/DHF (0.05%) is also similar to that of Au/DFH/0.1%) or even Au(DFH (2.5%) (Figure 7). We propose that the TOF values can be probably correlated better with the fraction of Au NPs whose size is smaller than 3 nm (Figure 7)

dx.doi.org/10.1021/am401489n | ACS Appl. Mater. Interfaces 2013, 5, 7160−7169

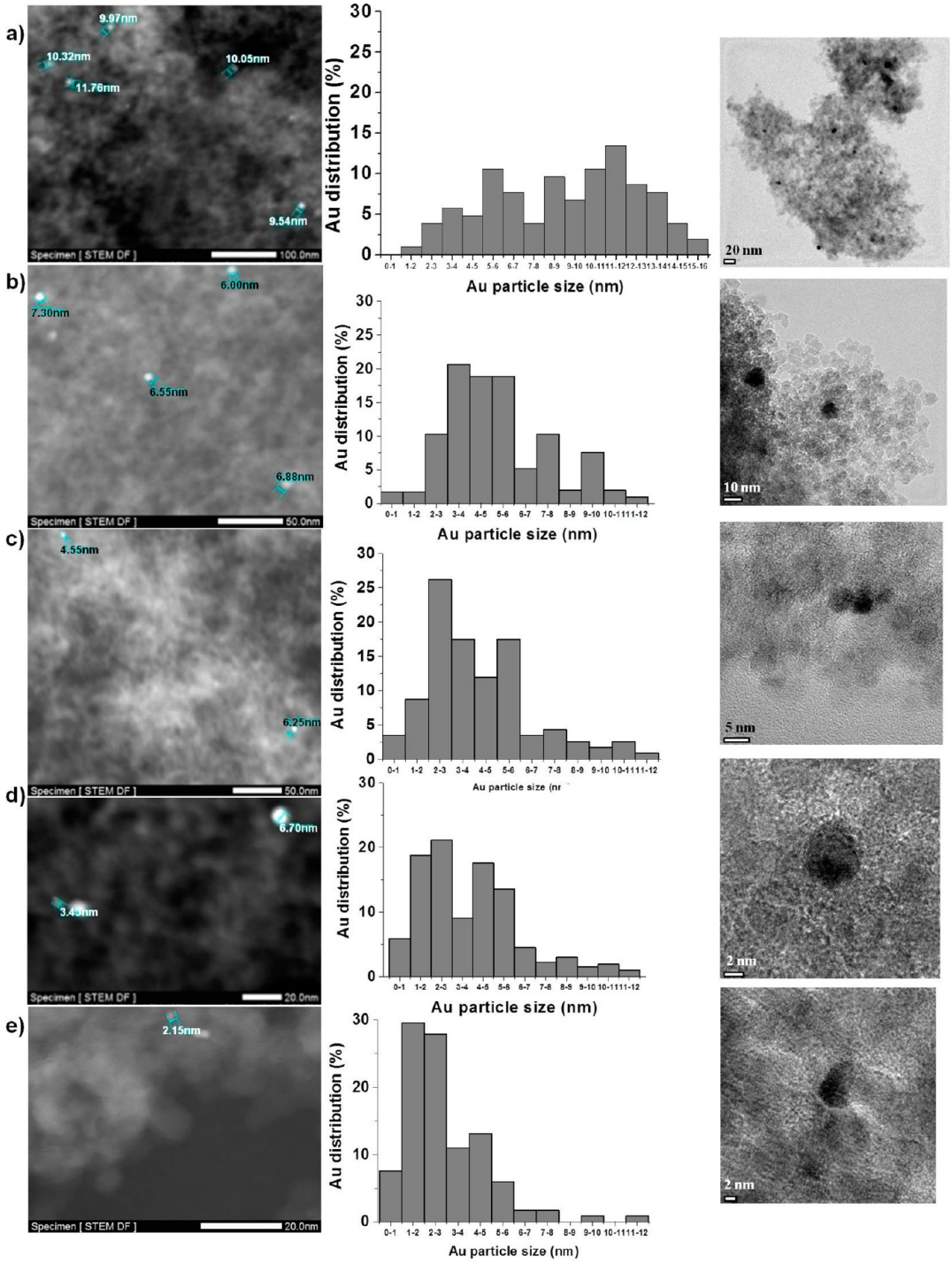

Figure 7. DF-STEM (left) and TEM (right) images and particle size distributions (middle) of (a) Au(0.5%)/DF, (b) Au(0.5%)/DFH, (c) Au(0.25%)/DFH, (d) Au(0.1%)/DFH, (e) Au(0.05%)/DFH. Note that for a more clear presentation of the images and particle size distribution the scale bars and X axis of each individual panel can be different from others.

and according to this, the gold loading on DFH support will exert a remarkable influence on both the TOF and percentage of small Au NPs. Thus, the most efficient sample, Au(0.05 wt %)/DFH, with highest phenol decomposition TOF value (943 h^{-1}) is the one with the highest fraction of Au NPs smaller than 3 nm (Figure 7e). In a simple way this rationalization implies that the very small Au NPs are basically the ones that contribute the most to the catalytic activity. It is also noteworthy from Figure 8 that the less efficient Au catalyst is the one in which the DF was used as support that corresponds to the largest average particle size of Au NPs.

Gold leaching from the heterogeneous Au(0.05%)/DFH catalyst to the solution working at pH 4 was less than 0.5% of the initial gold amount present in the solid. However, two additional reuse experiments using this catalyst resulted in a TOF decrease for phenol degradation from 943 h^{-1} for the fresh catalyst to 582 and 503 h^{-1} for the second and third uses, respectively. Due to the negligible gold leaching, we speculate that supported Au NPs suffer oxidation during the catalytic

dx.doi.org/10.1021/am401489n | ACS Appl. Mater. Interfaces 2013, 5, 7160−7169

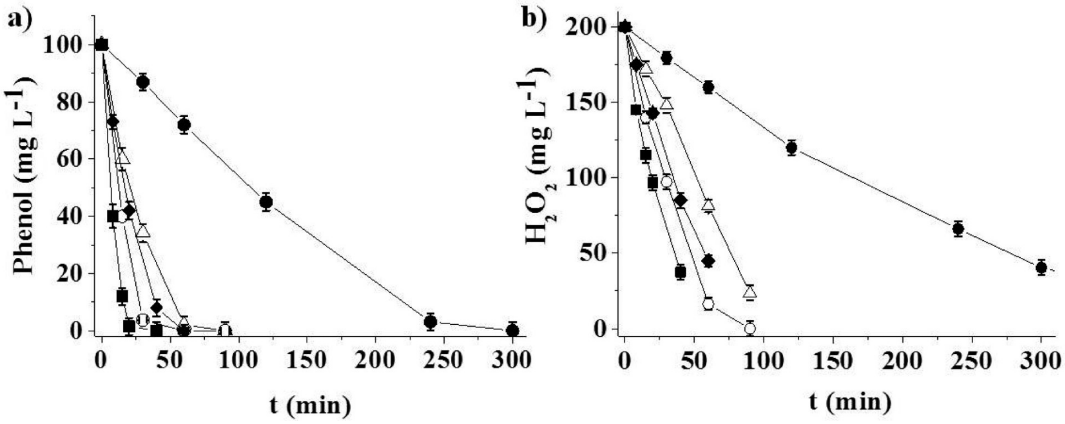

Figure 8. (a) Phenol disappearance and (b) H_2O_2 decomposition using different gold supported D catalysts. Legend: (■) Au(0.05%)/DFH, (○) Au(0.1%)/DFH, (◆) Au(0.25%)/DFH, (Δ) Au(0.5%)/DFH, (●) Au(0.5%)/DF. The error bars (see data points in the plot) have been estimated from two independent experiments.

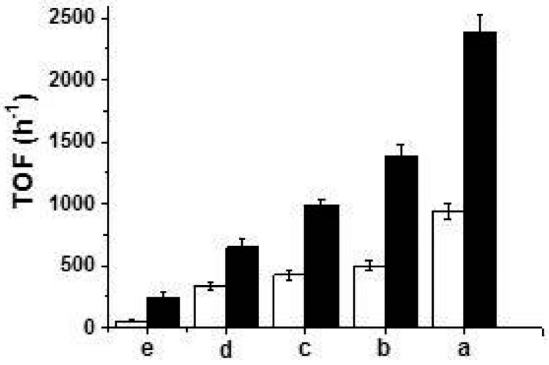

Figure 9. TOF for phenol degradation (white bars) and H_2O_2 decomposition (black bars) using different Au-supported D catalysts. Legend: (a) Au(0.05%)/DFH, (b) Au(0.1%)/DFH, (c) Au(0.25%)/DFH, (d) Au(0.5%)/DFH, (e) Au(0.5%)/DF. The error bars (see data points in the plot) have been estimated from two independent experiments.

cycles and then the catalyst decreases its initial activity. Effectively, when the gold catalyst before a reuse experiment is submitted to a reduction process by hot ethylene glycol, washed and, then, used for a new catalytic cycle, it recovers its initial catalytic activity. In this manner, three consecutive catalytic cycles were performed with almost constant TOF about 940 h^{-1} and final reaction time of 20 min. Importantly, after the three catalytic cycles the catalyst was characterized by DF-STEM and TEM measurements, observing a similar average of the Au NPs and particle size distribution (see Figure S5 in the Supporting Information).

To assess if the catalytic phenol degradation is assisted by natural sunlight and the reaction mechanism involves the generation of hydroxyl radicals, we performed two different controls. In one of them, the reaction was carried out under same conditions in the dark observing that the process was at least 25 times slower when the reaction was not exposed to the light. Figure 10 presents comparative time−conversion plots for these controls.

The intermediacy of •OH radicals was supported by determining the influence of DMSO on the reaction (Figure 10). It is known in the literature that DMSO is a •OH radical scavenger that can decrease degradation in those cases in which this specie is involved.[15] As it can be seen in this Figure 10, the presence of DMSO almost stops completely phenol degradation and exerts a notable influence on H_2O_2 decomposition.

Finally, we were interested in verifying that the previously characterized functional groups on the DFH support are

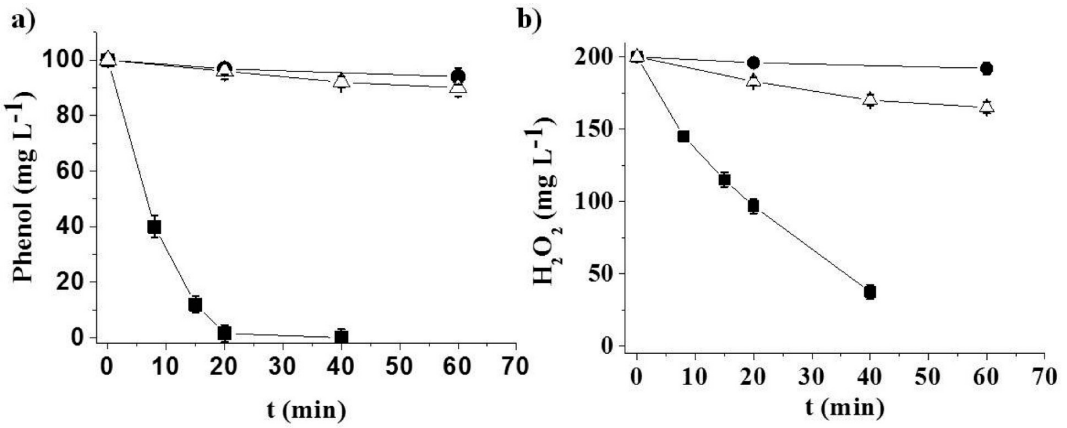

Figure 10. Time−conversion plots for phenol degradation (a) and H_2O_2 decomposition (b). Legend: (■) Au(0.05%)/DFH under natural Sunlight irradiation; (Δ) Au(0.05%)/DFH under Sunlight irradiation in the presence of DMSO; (●) Au(0.05%)/DFH under dark conditions. The error bars (see data points in the plot) have been estimated from two independent experiments.

responsible for both the formation of small Au NPs and the resulting high photocatalytic activity of the material. Aimed at providing experimental support to the claimed influence of the surface functional groups, we hypothesized that the removal of these surface hydroxyl groups, followed by subsequent Au NPs deposition would result in the formation of large NPs leading to low catalytic activity. Based on the TPD data for the DFH sample (Figure 3c) we submitted to the DFH support to N_2 flow at 700 °C for 30 min in order to remove surface oxygenated functional groups, rendering a new support devoid of surface hydroxyl denoted as DFH_N_2.

As expected, most of the oxygen functionalities of the original DFH sample were removed by this treatment as assessed by means of the ^{13}C NMR, FT-IR and TPD-MS data (see Figures S6–S8 in the Supporting Information) and elemental analysis (see Table S1 in the Supporting Information). Also, almost an identical BET surface area was measured for DFH support (286.1 $m^2\ g^{-1}$) before the thermal treatment and after it for the DFH_N_2 (289.0 $m^2\ g^{-1}$). Subsequent gold deposition on the DFH_N_2 support led to the Au (0.05%)/DFH_N_2 catalyst characterized by a broad Au NPs size distribution from 2 to 22 nm, with an average particle size of 11 nm (see Figure S9 in the Supporting Information). This particle size distribution is much broader than that estimated for the Au(0.05%)/DFH sample (Figure 7e). As expected in view of the low Au percentage on the solid, powder XRD of the Au (0.05%)/DFH_N_2 sample does not clearly exhibit the characteristic Au diffraction peaks (see Figure S10 in the Supporting Information). As expected, negligible photocatalytic activity of the sample for both phenol degradation and H_2O_2 decomposition was observed under the studied reaction conditions (see Figure S11 in the Supporting Information). These results support the role of hydroxyl groups in the D support anchoring Au species to obtain in a subsequent step small Au NPs with narrow particle size distribution and, consequently, high catalytic activity.

4. CONCLUSIONS

When commercial D material is submitted to Fenton oxidation in addition to hydroxyl groups also carboxylic groups, esters and anhydrides are simultaneously formed. We have found that the heterogeneity in the composition of the surface functional groups plays an adverse effect, being responsible for the formation of larger Au NPs as revealed by TEM. Hydrogen reduction at high temperatures removes most of the carboxylic acid groups, esters, and lactones from the Fenton-treated D surface, as evidenced by TPD. We have found that this treatment is beneficial for the catalytic activity due to the fact that this hydroxylated surface is more appropriate to obtain smaller-sized Au NPs. Thus, we have shown that modifying the nature of the functional groups present on the surface of D NPs, optimization of the catalytic activity can be achieved.

■ ASSOCIATED CONTENT

Supporting Information

C1s and O1s XPS of DF and DFH samples (Figure S1); DF-STEM image and X-EDS spectrum of Au(0.05%)/DFH sample (Figure S2); TEM images of the different gold catalysts under study (Figure S3); DF-STEM images of the different gold catalysts under study (Figure S4); TEM and DF-STEM images and particle size distributions of Au(0.05%)/DFH after three uses (Figure S5); ^{13}C NMR spectra of commercial D, DFH, and DFH_N_2 samples (Figure S6); FT-IR of DFH and DFH_N_2 samples (Figure S7); Comparison of CO and CO_2 evolution obtained from TPD-MS for DFH and DFH_N_2 samples (Figure S8); TEM and DF-STEM images and particle size distributions of Au(0.05%)/DFH_N_2 (Figure S9); XRD diffractogram of Au(0.05%)/DFH_N_2 (Figure S10); phenol degradation and H_2O_2 decomposition under natural sunlight irradiation (Figure S11); elemental analysis and S_{BET} of DFH_N_2 (Table S1). This material is available free of charge via the Internet at http://pubs.acs.org.

■ AUTHOR INFORMATION

Corresponding Author

*E-mail: hgarcia@qim.upv.es (H.G.); sernaol@doctor.upv.es (S.N.).

Funding

Financial support by the Spanish Ministry of Economy and Competitiveness (MINECO, Severo Ochoa program and CTQ 2012–32315), Universidad Politécnica de Valencia (PAID-06–11, n° 2095) and Generalitat Valenciana (Prometeo 2013/014 and GV/2013/040).

Notes

The authors declare no competing financial interest.

■ ACKNOWLEDGMENTS

S.N. thanks the UPV for a lecturer contract.

■ REFERENCES

(1) Neyens, E.; Baeyens, J. *J. Hazard. Mater.* **2003**, *98*, 33–50.
(2) Pera-Titus, M.; García-Molina, V.; Baños, M. A.; Giménez, J.; Esplugas, S. *Appl. Catal., B* **2004**, *47*, 219–256.
(3) Pignatello, J. J.; Oliveros, E.; Mackay, A. *Crit. Rev. Environ. Sci. Technol.* **2006**, *36*, 1–84.
(4) Dhakshinamoorthy, A.; Navalon, S.; Alvaro, M.; Garcia, H. *ChemSusChem* **2012**, *5*, 46–64.
(5) Navalon, S.; Alvaro, M.; Garcia, H. *Appl. Catal., B* **2010**, *99*, 1–26.
(6) Navalon, S.; Dhakshinamoorthy, A.; Alvaro, M.; Garcia, H. *ChemSusChem* **2011**, *4*, 1712–1730.
(7) Herney-Ramirez, J.; Vicente, M. A.; Madeira, L. M. *Appl. Catal., B* **2010**, *98*, 10–26.
(8) Martin, R.; Navalon, S.; Alvaro, M.; Garcia, H. *Appl. Catal., B* **2010**, *103*, 246–252.
(9) Navalon, S.; Martin, R.; Alvaro, M.; Garcia, H. *Angew. Chem., Int. Ed.* **2010**, *49*, 8403–8407.
(10) Martin, R.; Navalon, S.; Delgado, J. J.; Calvino, J. J.; Alvaro, M.; Garcia, H. *Chem.—Eur. J.* **2011**, *17*, 9494–9502.
(11) Navalon, S.; Miguel, M. d.; Martin, R.; Alvaro, M.; Garcia, H. *J. Am. Chem. Soc.* **2011**, *133*, 2218–2226.
(12) Hoffmann, M. R.; Martin, S. T.; Choi, W.; Bahnemann, D. W. *Chem. Rev.* **1995**, *95*, 69–96.
(13) Martin, S. T.; Herrmann, H.; Choi, W.; Hoffmann, M. R. *J. Chem. Soc., Faraday Trans* **1994**, *90*, 3315–3322.
(14) Martin, S. T.; Herrmann, H.; Hoffmann, M. R. *J. Chem. Soc., Faraday Trans.* **1994**, *90*, 3323–3330.
(15) Navalon, S.; Martin, R.; Alvaro, M.; Garcia, H. *ChemSusChem* **2011**, *4*, 650–657.
(16) Dhakshinamoorthy, A.; Navalon, S.; Sempere, D.; Alvaro, M.; Garcia, H. *ChemCatchem* **2013**, *5*, 241–246.
(17) Carroll, K. J.; Reveles, J. U.; Shultz, M. D.; Khanna, S. N.; Carpenter, E. E. *J. Phys. Chem. C* **2011**, *115*, 2656–2664.
(18) Joseyphus, R. J.; Shinoda, K.; Kodama, D.; Jeyadevan, B. *Mater. Chem. Phys.* **2010**, *123*, 487–493.
(19) López-Santos, C.; Yubero, F.; Cotrino, J.; González-Elipe, A. R. *Diamond Relat. Mater.* **2011**, *20*, 49–56.
(20) Abad, A.; Corma, A.; García, H. *Chem.—Eur. J.* **2008**, *14*, 212–222.

(21) Figueiredo, J. L.; Pereira, F. R.; Freitas, M. M. A.; Órfao, J. J. M. *Carbon* **1999**, *37*, 1379−1389.
(22) Osswald, S.; Yushin, G.; Mochalin, V.; Kucheyev, S. O.; Gogotsi, Y. *J. Am. Chem. Soc.* **2006**, *128*, 11635−11642.
(23) Chen, X.; Liu, L.; Yu, P. Y.; Mao, S. S. *Science* **2011**, *331*, 746−750.
(24) Zhou, J.-H.; Sui, Z.-J.; Zhu, J.; Li, P.; Chen, D.; Dai, Y.-C.; Yuan, W.-K. *Carbon* **2007**, *45*, 785−796.
(25) Girard, H. A.; Arnault, J. C.; Perruchas, S.; Saada, S.; Gacoin, T.; Boilot, J.-P.; Bergonzo, P. *Diamond Relat. Mater.* **2010**, *19*, 1117−1123.
(26) Zeppilli, S.; Arnault, J. C.; Gesset, C.; Bergonzo, P.; Polini, R. *Diamond Relat. Mater.* **2010**, *19*, 846−853.
(27) Wang, Z.; Zhang, Q.; Kuehner, D.; Ivaska, A.; Niu, L. *Green Chem.* **2008**, *10*, 907−909.
(28) Stratakis, M.; Garcia, H. *Chem. Rev.* **2012**, *112*, 4469−4506.
(29) Astruc, D.; Lu, F.; Aranzaes, J. R. *Angew. Chem., Int. Ed.* **2005**, *44*, 7852−7872.